



ARTICLE

DOI: 10.1038/s41467-018-05928-5

OPEN

Structural basis for importin alpha 3 specificity of W proteins in Hendra and Nipah viruses

Kate M. Smith¹, Sofiya Tsimbalyuk¹, Megan R. Edwards², Emily M. Cross¹, Jyoti Batra², Tatiana P. Soares da Costa³, David Aragão ⁴, Christopher F. Basler ² & Jade K. Forwood¹

Seven human isoforms of importin α mediate nuclear import of cargo in a tissue- and isoform-specific manner. How nuclear import adaptors differentially interact with cargo harbouring the same nuclear localisation signal (NLS) remains poorly understood, as the NLS recognition region is highly conserved. Here, we provide a structural basis for the nuclear import specificity of W proteins in Hendra and Nipah viruses. We determine the structural interfaces of these cargo bound to importin $\alpha 1$ and $\alpha 3$, identifying a 2.4-fold more extensive interface and > 50-fold higher binding affinity for importin $\alpha 3$. Through the design of importin $\alpha 1$ and $\alpha 3$ chimeric and mutant proteins, together with structures of cargo-free importin $\alpha 1$ and $\alpha 3$ isoforms, we establish that the molecular basis of specificity resides in the differential positioning of the armadillo repeats 7 and 8. Overall, our study provides mechanistic insights into a range of important nucleocytoplasmic transport processes reliant on isoform adaptor specificity.

¹School of Biomedical Sciences, Charles Sturt University, Wagga Wagga, NSW 2678, Australia. ²Center for Microbial Pathogenesis, Institute for Biomedical Sciences, Georgia State University, Atlanta, GA 30303, USA. ³Department of Biochemistry and Genetics, La Trobe Institute for Molecular Science, La Trobe University, Melbourne, VIC 3086, Australia. ⁴Australian Synchrotron, Australian Nuclear Science and Technology Organisation, 800 Blackburn Road, Clayton, VIC 3168, Australia. These authors contributed equally: Kate M. Smith, Sofiya Tsimbalyuk, Megan R. Edwards. These authors jointly supervised this work: Christopher F. Basler, Jade K. Forwood. Correspondence and requests for materials should be addressed to C.F.B. (email: cbasler@gsu.edu) or to J.K.F. (email: jforwood@csu.edu.au)

Active transport of proteins from the cytoplasm to the nucleus is mediated by a family of nuclear transport receptors known as importins (or karyopherins), together with a number of ancillary proteins including nucleoporins and Ran^{1–3}. The classical nuclear import pathway is best understood, and is initiated by recognition of proteins that contain a classical nuclear localisation sequence (NLS) by importin α ⁴. This complex is transported through the nuclear pore complex by importin β , involving interactions with FG repeat regions contained within nucleoporin proteins^{5,6}. Once the complex has traversed the nuclear envelope, RanGTP dissociates the complex, and the import receptors are recycled back to the cytoplasm to perform further rounds of transport^{7–10}. Importin α is constructed from an N-terminal importin β -binding (IBB) domain and a C-terminal NLS binding domain featuring ten armadillo (ARM)-repeat motifs¹¹. Most commonly, the cargo NLS binds on the concave site of the ARM repeats and involves interactions at either the major site, through ARM repeats 2–4 in the case of classical monopartite NLSs (e.g., SV40T-ag¹²), the minor site involving ARM repeats 6–8 (e.g., human phospholipid scramblase¹³, TPX2¹⁴) or both the major and minor sites in the case of classical bipartite NLSs (e.g., nucleoplasmin¹²). Although this process has been well characterised for the importin $\alpha 1$ adaptor protein, many nuclear proteins exhibit specificity for other importin α isoforms, and the molecular basis for this specificity is understood poorly. Complicating our understanding of how importin α isoforms exhibit specificity, the seven importin α isoforms are highly conserved in the regions that mediate NLS binding. Establishing how nuclear cargo are recognised in an isoform-specific manner is important for understanding many key regulatory processes including cell differentiation, cancer and viral infection. For example, both RCC1 (the exchange factor of Ran that regulates the directionality of nuclear transport) and HIV-1 integrase (responsible for integrating the HIV-1 genome into the DNA of an infected cell) bind specifically to importin $\alpha 3$ ^{15,16}. STAT1, a signalling molecule in the innate immune system response, binds specifically to the convex C-terminal surface of importin $\alpha 5$, $\alpha 6$ and $\alpha 7$ ^{17,18}. The avian influenza PB2 viral polymerase subunit, which is a major virulence determinant, has isoform specificity for importin $\alpha 3$ in avian hosts and importin $\alpha 7$ in mammalian hosts, providing a kinetic advantage owing to lower importin α autoinhibition by the importin β binding domain¹⁹.

The W protein of Nipah virus (NiV) is recognised specifically by importin $\alpha 3$, which occurs through an NLS in the unique C-terminal domain^{20,21}, however, the basis of this specificity remains unclear. HeV and NiV are recently emergent, zoonotic pathogens of the *Henipavirus* genus in the *Paramyxoviridae* family. These viruses use bats of the *Pteropus* genus as reservoir hosts but cause infections in humans with a high rate of fatality (~60%)²². The viruses are non-segmented, negative-sense RNA viruses and encode six genes, five of which encode a single protein, whereas, the sixth gene, P, encodes four proteins: P, V, W and C. Of these, P, V and W share a common N-terminal domain, but differ within the C-terminal domain owing to frame-shifting that results from insertion of non-template encoded nucleotides into P gene transcripts^{23–25}. This results in proteins that have different functions and cellular locations, with only the W protein displaying steady-state nuclear localisation owing to a C-terminally located NLS^{20,26}. In the context of NiV infection, the nonstructural W protein plays an important role in virulence^{27–29}. It has been demonstrated to antagonise innate antiviral defences by blocking interferon-induced gene expression and by preventing expression of type I IFNs, with nuclear localisation shown to be important for the latter function^{20,30}. A recent study has identified additional host targets of NiV W,

including the PRP19 complex, for which the nuclear localisation of W appears to be required for the interaction³¹.

Previous reports have demonstrated specificity of the importin $\alpha 3$ adaptor for the NiV W protein, however, like most cargo, the basis for this specificity is unknown^{20,32}. Here, we establish key differences in the binding interface of W proteins with importin $\alpha 1$ and $\alpha 3$, providing insights into adaptor specificity. We use mutagenesis and chimeras of importin $\alpha 1$ and $\alpha 3$ to confirm the importance of these differences and show that the C-terminal ARM repeats 7 and 8 of importin $\alpha 3$ are important for specificity as their conformation in importin $\alpha 3$ allows for an extensive binding interface not possible in importin $\alpha 1$. These insights extend our understanding of adaptor specificity and establish how important nuclear cargo proteins are imported in an isoform-specific manner.

Results

Henipavirus W preferentially bind importin $\alpha 3$ and $\alpha 4$. The W proteins of henipaviruses share a common N-terminal domain with P and V proteins, but have a unique NLS bearing C-terminal domain that is recognised preferentially by importins $\alpha 3$ and $\alpha 4$ (KPNA4 and KPNA3), rather than the better characterised importin $\alpha 1$ (KPNA2) (Fig. 1a and Supplementary Fig. 1A)²⁰. To confirm this, and assess W binding against a more extensive range of importin α isoforms, we performed co-immunoprecipitation assays against respective importins and probed for the presence of HeV and NiV W. We found that both HeV and NiV W bound preferentially to importin $\alpha 3$ and $\alpha 4$, but not importin $\alpha 1$, $\alpha 5$, $\alpha 6$ or $\alpha 7$ (Fig. 1b and Supplementary Fig. 2). These importin α s extend across all subfamilies (Supplementary Fig. 1B), confirming that the W protein binds specifically to members of importin α subfamily-2.

To determine the binding affinities between importin $\alpha 3$ and Henipavirus W proteins, as well as confirm a direct interaction, the C-terminal NLS domain of the W protein from both HeV and NiV were cloned as a glutathione S-transferases (GST) fusion protein and assessed for importin α binding by isoforms from representative subfamilies. From enzyme-linked immunosorbent assay (ELISA) measurements, we found that importin $\alpha 3$ bound with high affinity to the W protein from both HeV and NiV (19.9 nM and 14.4 nM, respectively), whereas importin $\alpha 1$ and $\alpha 7$ bound with much lower affinity (1.4 μ M and 1.5 μ M, respectively, to HeV W; and 1.5 μ M and 1.1 μ M, respectively, to NiV W) (Fig. 1c; Supplementary Table 1). We found comparable binding using microscale thermophoresis (MST) assays, with importin $\alpha 3$ binding NiV W protein with high affinity (4.4 nM), whereas importin $\alpha 1$ and $\alpha 7$ displayed a much lower affinity (681 and 696 nM, respectively) (Fig. 1d; Supplementary Table 2). Together these data establish a direct, high-affinity interaction of the W proteins from henipaviruses for importin $\alpha 3$ compared with other importin α subfamilies.

Structural basis for importin α isoform specificity to W. To establish the mechanism and molecular basis of the isoform-specific differences, we used X-ray crystallography to determine the structural interface of both the high-affinity importin $\alpha 3$ interaction and the low-affinity importin $\alpha 1$ interaction. Structures were determined for importin $\alpha 3$ and $\alpha 1$ bound to both the HeV W and NiV W C-terminal NLS-bearing domain (Fig. 2 and Fig. 3, respectively). Crystals of the importin $\alpha 1$:HeV W complex had P2₁2₁2₁ symmetry and diffracted to 2.2 Å resolution. The asymmetric unit (ASU) contained one importin $\alpha 1$ chain bound to a single HeV W chain, in which residues 434–441 were bound to importin $\alpha 1$. The interaction was mediated by 15 hydrogen bonds, one salt bridge interaction, and buried a surface area of 683.5 Å² (see Table 1 for full

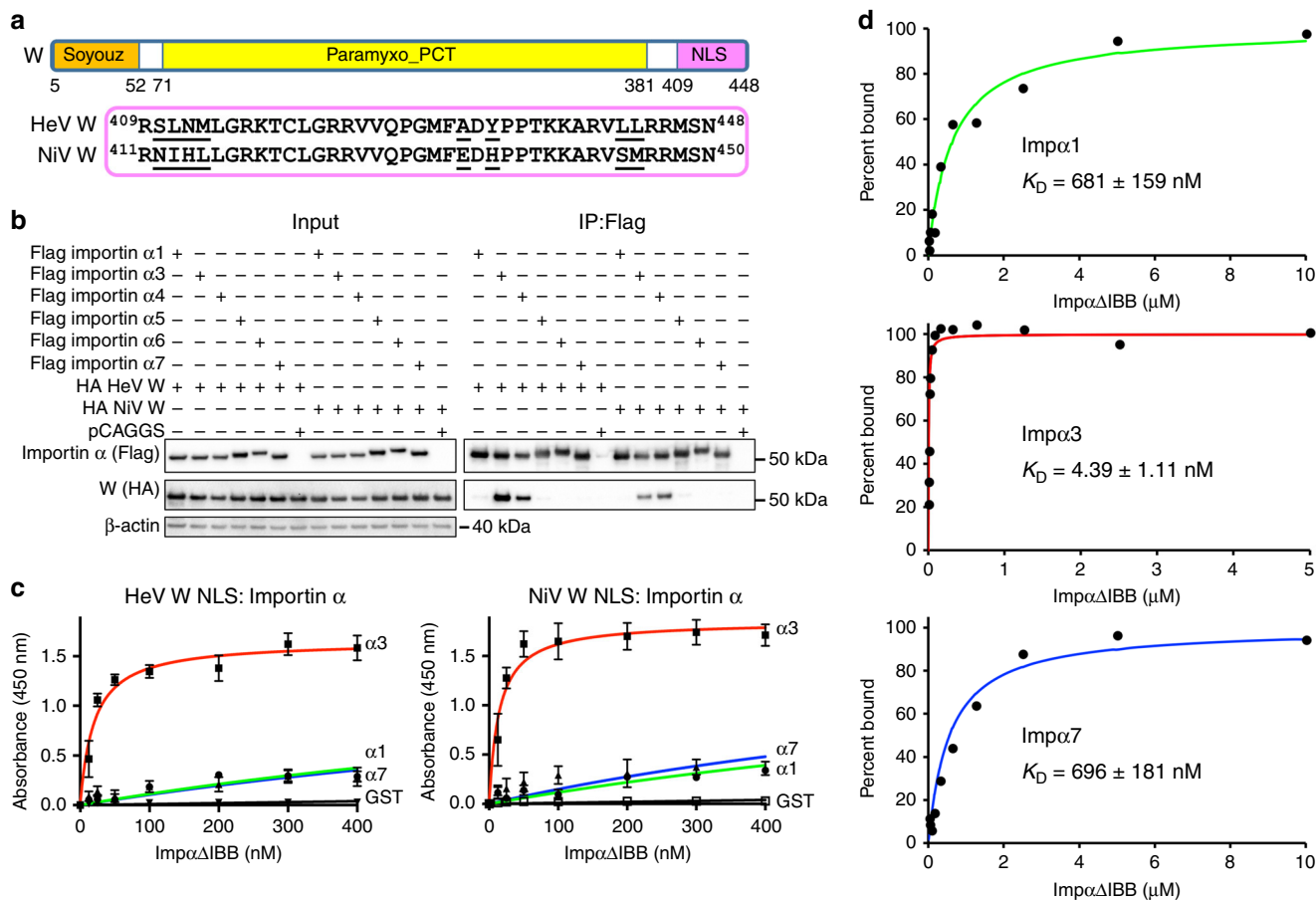


Fig. 1 Binding of Henipavirus W proteins to importins. The NLS regions of Henipavirus W proteins bind with high affinity and specificity to the importin α 2 subfamily containing importin α 3 and α 4. **a** The W proteins contain the Soyouz module moiety (Soyouz) and PCT disordered (Paramyxo_PCT) regions, which are conserved across paramyxovirus phosphoproteins. However, the W proteins of HeV and NiV W also possess a unique C terminus compared with other P gene products and contain an NLS that mediates translocation of W into the nucleus. **b** HeV W and NiV W interact with importin α 3 and α 4. Co-immunoprecipitation assay performed with Flag antibody on lysates of HEK293T cells expressing Flag-tagged importin α 1, α 3, α 4, α 5, α 6, α 7 and HA-tagged full length HeV W and NiV W, as indicated. Western blots were performed for HA and Flag. WCL, whole cell lysate; IP, immunoprecipitation. pCAGGS denotes empty vector control. **c** The NLS region of HeV W and NiV W interact with high affinity to importin α 3. An ELISA was performed using GST-W (GST as a negative control) proteins coated on 96-well plates, and binding of 6xHis-tagged importin α 1, α 3, α 7 assessed using an anti-6xHis HRP antibody. Error bars show the S.E.M for three replicates. **d** MST assay confirms high affinity binding of importin α 3 to the NLS region of NiV W proteins, and comparatively lower affinity binding to importin α 1 and α 7

data collection and refinement statistics and Supplementary Table 3 for a detailed list of the interactions).

The structure of the importin α 3:HeV W complex was determined in three different space groups (Table 2), with all crystals exhibiting highly similar structures (r.m.s.d < 0.35; Supplementary Fig. 3) and containing one HeV W NLS chain bound to a single importin α 3 chain (the highest resolution structure of 1.6 Å will be used for further discussion and analysis). In contrast to the importin α 1:HeV W complex, importin α 3 bound a more extensive region of the HeV W C-terminal domain NLS (residues 419–444) and showed a more extensive array of hydrogen bonds (31 vs 15), seven salt bridge interactions (7 vs 1), and a greater buried surface area (1616.9 vs 683.5 Å²); (see Supplementary Table 4 and Supplementary Table 5 for a detailed list of interactions and summary comparisons, respectively).

To test whether the same binding patterns were present in the NiV W protein, we examined the binding determinants of importin α :NiV W complexes using the same approach. We observed binding patterns that were very similar to those seen with HeV W for both importin α 1 and α 3 (Fig. 3). Crystals of the importin α 1:

NiV W complex (that had P₂1₂1 symmetry and diffracted to 2.1 Å resolution) bound residues 436–443 of the NiV W C-terminal domain. In comparison, the importin α 3:NiV W complex had P1₂1 symmetry, diffracted to 2.3 Å resolution, and showed more extensive binding, with residues 421–446 bound to importin α 3. The binding interface was also similar to HeV W, with the importin α 1:NiV W complex mediated by 15 hydrogen bonds, one salt bridge interaction, and a buried surface area of 688.7 Å². The importin α 3:NiV W interface was mediated through 31 hydrogen bonds, seven salt bridge interactions, and buried 1591.8 Å² of surface area. These results indicate that the interaction of the henipavirus W proteins with importins is highly conserved.

Establishing the structural interface between importin α 1 and α 3 in both HeV W and NiV W highlighted key differences in importin recognition and gave insights into isoform specificity. Notably, despite binding the same region of HeV W and NiV W, importin α 3 exhibited a 2.4-fold more extensive interaction buried surface area than importin α 1, with 16 additional hydrogen bonds, and six additional salt bridge interactions, consistent with its >50-fold higher affinity. Both W proteins

Table 1 Data collection and refinement statistics for importin $\alpha 1$ structures

	Imp $\alpha 1^a$	NiV W Imp $\alpha 1^a$	HeV W Imp $\alpha 1^a$
<i>Data Collection</i>			
Wavelength (Å)	0.9537	0.9537	0.9537
Space group	P 2 ₁ 2 ₁ 2 ₁	P 2 ₁ 2 ₁ 2 ₁	P 2 ₁ 2 ₁ 2 ₁
Cell dimensions			
<i>a</i> , <i>b</i> , <i>c</i> (Å)	78.5, 90.0, 100.7	77.9, 88.8, 97.6	79.0, 89.3, 100.4
α , β , γ (°)	90, 90, 90	90, 90, 90	90, 90, 90
Resolution (Å)	24.54–2.50 (2.60–2.50)	29.61–2.10 (2.16–2.10)	19.76–2.20 (2.28–2.20)
R_{pim}	0.061 (0.365)	0.033 (0.253)	0.029 (0.147)
Mean <i>I</i> / σ (<i>I</i>)	10.2 (2.9)	11.7 (2.4)	18.5 (5.4)
CC _{1/2}	0.989 (0.751)	0.998 (0.814)	0.999 (0.928)
Total reflections	154,003 (17460)	136,253 (11369)	208,967 (18156)
Unique reflections	24,805 (2822)	38,272 (3193)	36,721 (3139)
Completeness (%)	98.6 (100)	96 (97.8)	99.8 (100)
Redundancy	6.2 (6.2)	3.6 (3.6)	5.7 (5.8)
Wilson <i>B</i> -factor	26.4	31.8	22.6
<i>Refinement</i>			
Resolution (Å)	24.54–2.50	28.79–2.10	19.76–2.20
Reflections used in			
Refinement	24,772 (2478)	38,216 (3843)	36,662 (3611)
R_{free}	1262 (133)	1864 (172)	1861 (176)
R_{work}	0.1910 (0.2227)	0.1854 (0.2690)	0.1915 (0.2257)
R_{free}	0.2129 (0.2572)	0.2032 (0.3062)	0.2121 (0.2774)
Number of non-hydrogen atoms	3361	3555	3431
Macromolecules	3244	3306	3306
Protein residues	426	434	434
<i>B</i> factors	42.49	51.14	38.89
Protein	42.66	51.31	38.98
Water	37.95	48.89	36.67
R.M.S. deviations			
Bond lengths (Å)	0.004	0.005	0.003
Bond angles (°)	0.59	0.73	0.62
Ramachandran plot (%)			
Favoured	99	99	98
Allowed	1.4	1.4	1.9
Outliers	0	0	0
Rotamer outliers (%)	1.1	1.1	0.27
Clash score	0.46	0.90	1.19

^aValues in parentheses are for highest resolution shell

region of importin $\alpha 3$ is unlikely to play a role in cargo containing an NLS in the C terminus of the protein (as the NLS ends before reaching the hinge region), the positioning of ARM repeats 1–3 could play a role in the binding of proteins harbouring an NLS at the N terminus, such as RCC1 (see Discussion).

Chimera of importin $\alpha 1$ ARMs 1–5: $\alpha 3$ ARMs 6–10 retains binding. To test our hypothesis that the positioning of ARM repeats 7 and 8, located in the C terminus of importin $\alpha 3$, mediate the isoform specificity for *W* protein, we examined whether chimeras comprised of importin $\alpha 1$ and importin $\alpha 3$ could mediate binding to *W* proteins (Fig. 7a). We found that a chimera comprised of the N terminus of importin $\alpha 1$ (IBB domain and ARMs 1–5) and the C terminus of importin $\alpha 3$ (ARMs 6–10) (importin $\alpha 1^{ARM1-5}:\alpha 3^{ARM6-10}$) bound *W*, whereas the reverse chimera comprised of importin $\alpha 3$ IBB ARMs 1–5 and importin $\alpha 1$ ARMs 6–10 (importin $\alpha 3^{ARM1-5}:\alpha 1^{ARM6-10}$) did not pull-down *W* (Fig. 7b). These results support the structural data that the C-terminal domain of importin $\alpha 3$ mediates isoform specificity for the *W* protein. Moreover, the importin $\alpha 1^{ARM1-5}:\alpha 3^{ARM6-10}$ bound with 8.3 nM affinity to HeV *W*, and 4.7 nM

affinity to NiV *W*, comparable to the binding affinity of importin $\alpha 3$ (Supplementary Fig. 5). To further test the involvement of ARMs 7 and 8 in mediating specificity, we designed an importin $\alpha 3$ mutant based on the structural data to disrupt interactions in ARMs 7/8 (N348 A/N352A/E387A/N394A), and found a marked reduction in binding to both HeV and NiV *W* proteins (Fig. 7c). Confirming their functionality, both the importin $\alpha 1^{ARM1-5}:\alpha 3^{ARM6-10}$ chimera and importin $\alpha 3$ ARMs 7/8 mutant retained the ability to bind to the SV40Tag classical NLS (Supplementary Fig. 6). The importin $\alpha 3^{ARM1-5}:\alpha 1^{ARM6-10}$ formed inclusion bodies during overexpression and could not be purified. These results, together with the structural data, suggest that the positioning of the C-terminal ARM repeats 7 and 8 are important for mediating isoform specificity of henipavirus *W* proteins.

Discussion

In this study, we present high-resolution structures of importin α isoform adaptors bound to the NLS regions of HeV *W* and NiV *W*, providing insights into the molecular basis of importin α isoform specificity. We found that HeV *W* and NiV *W* proteins bind importin $\alpha 3$ preferentially, and that these NLS regions

Table 2 Data collection and refinement statistics for importin $\alpha 3$ structures

	Imp $\alpha 3^a$	NiV W Imp $\alpha 3^a$	HeV W Imp $\alpha 3^a$ crystal form 1	HeV W Imp $\alpha 3^a$ crystal form 2	HeV W Imp $\alpha 3^a$ crystal form 3
<i>Data collection</i>					
Wavelength (Å)	0.9537	0.9537	0.9537	0.9537	0.9537
Space group	P 1 2 ₁ 1	P 1 2 ₁ 1	P 1 2 ₁ 1	P 1 2 ₁ 1	P 2 ₁ 2 ₁ 2 ₁
Cell dimensions					
<i>a</i> , <i>b</i> , <i>c</i> (Å)	47.1, 53.2, 91.3	47.7, 65.6, 73.9	47.4, 65.7, 74.2	48.1, 60.0, 89.9	48.2, 59.0, 169.3
α , β , γ (°)	90, 92.87, 90	90, 99.79, 90	90, 99.76, 90	90, 97.85, 90	90, 90, 90
Resolution (Å)	19.81–2.30 (2.38–2.30) ^a	38.21–2.30 (2.38–2.30)	19.84–1.6 (1.63–1.60)	19.95–2.20 (2.27–2.20)	29.49–2.30 (2.38–2.30)
R _{pim}	0.086 (0.304)	0.087 (0.274)	0.061 (0.174)	0.081 (0.369)	0.032 (0.077)
Mean <i>I</i> / σ (<i>I</i>)	11.3 (1.8)	8.6 (3.5)	7.1 (3.3)	9.6 (3.7)	17.1 (8.8)
CC _{1/2}	0.977 (0.785)	0.781 (0.817)	0.989 (0.899)	0.974 (0.446)	0.997 (0.973)
Total reflections	105,917 (11,952)	46,617 (4355)	254,011 (12,863)	90,676 (7765)	286,394 (27,948)
Unique reflections	19,290 (1942)	19,881 (1953)	58,984 (2917)	25,833 (2232)	22,252 (2139)
Completeness (%)	95 (98.2)	98.9 (99.2)	99.4 (99.6)	99.6 (99.8)	100 (100)
Redundancy	5.5 (6.2)	2.3 (2.2)	4.3 (4.4)	3.5 (3.5)	12.9 (13.1)
Wilson <i>B</i> -factor	37.1	20.4	10.7	15.5	15.1
<i>Refinement</i>					
Resolution (Å)	19.48–2.30	36.75–2.30	19.58–1.60	19.95–2.20	29.36–2.30
Reflections used in					
Refinement	19,147 (1978)	19,788 (1980)	58,886 (5838)	25,804 (2546)	22,192 (2161)
<i>R</i> _{free}	937 (91)	989 (94)	2894 (275)	1227 (115)	1119 (123)
<i>R</i> _{work}	0.2500 (0.2662)	0.1991 (0.2177)	0.1711 (0.1978)	0.1859 (0.2606)	0.1771 (0.1929)
<i>R</i> _{free}	0.2684 (0.3212)	0.2223 (0.2917)	0.1962 (0.2421)	0.2148 (0.2946)	0.2182 (0.2578)
Number of non-hydrogen atoms	3210	3592	3738	3678	3624
Macromolecules	3206	3400	3400	3419	3419
Protein residues	415	440	440	442	442
<i>B</i> factors	55.53	30.56	18.57	30.72	27.54
Protein	55.56	30.59	17.77	30.47	27.46
Water	35.29	30.04	26.57	33.99	28.91
R.M.S. deviations					
Bond lengths (Å)	0.005	0.006	0.015	0.003	0.006
Bond angles (°)	1.03	0.75	1.21	0.54	0.71
Ramachandran plot (%)					
Favoured	99	98	99	98	98
Allowed	1.2	2.1	1.4	2.3	2.1
Outliers	0	0	0	0	0
Rotamer outliers (%)	0.83	0.26	0.52	0.52	0.52
Clash score	3.57	1.03	1.76	0.87	1.89

^aValues in parentheses are for highest resolution shell

interact with higher affinity over other importin α subfamilies. Using structural approaches, we identified key features that account for adaptor specificity. We found that the isoform specificity was localised to the C-terminal ARM repeats 7 and 8, and that the positioning of these domains was an important determinant for mediating specificity.

Although numerous studies have reported specificity of nuclear adaptors for a wide range of cargo^{19,34–37} and associated function of these interactions in many diseases³⁶, the mechanism(s) behind NLS adaptor specificity has remained elusive. Recently, one study described the specificity of the RCC1 factor for importin $\alpha 3$, highlighting that additional residues outside the NLS were important for maintaining specificity¹⁵. A comparison between the mechanism presented in the RCC1 study and our study, highlights a number of important differences. The study by Sankhala et al.¹⁵ indicated that the NLS of RCC1 binds in the major binding site of ARMS 2–4 of both importin $\alpha 1$ and $\alpha 3$, with additional interactions occurring at the N terminus of importin $\alpha 3$ ARM repeats 1–4 and the β -propeller region of RCC1,

mediated by flexibility and rotation of importin $\alpha 3$ in ARM repeats 1–2. This mechanism of isoform specificity is well suited to cargo containing NLSs at the N terminus, and our structural data of the unbound and NLS-bound forms of importin $\alpha 3$ supports this model. This mechanism is distinct, however, from that governing specificity for cargo such as the W proteins in this study, where the NLSs are located at the C terminus because the protein interface would not extend past the N terminus of ARM repeats 2–4. Thus, it may be possible that isoform specificity of cargo containing N-terminal NLSs may reside through differential interaction of the N-terminal ARM repeats, whereas cargo bearing C-terminal NLSs may show specificity through differential interaction with the C terminus of importins, as demonstrated in this study. Although further work will be needed to establish how extensive these rules are, it is likely that different mechanisms may govern isoform specificity, dependent upon the position of the NLS within the cargo.

The findings of our study are distinct from mechanisms that have been previously hypothesised. The IBB domain has been

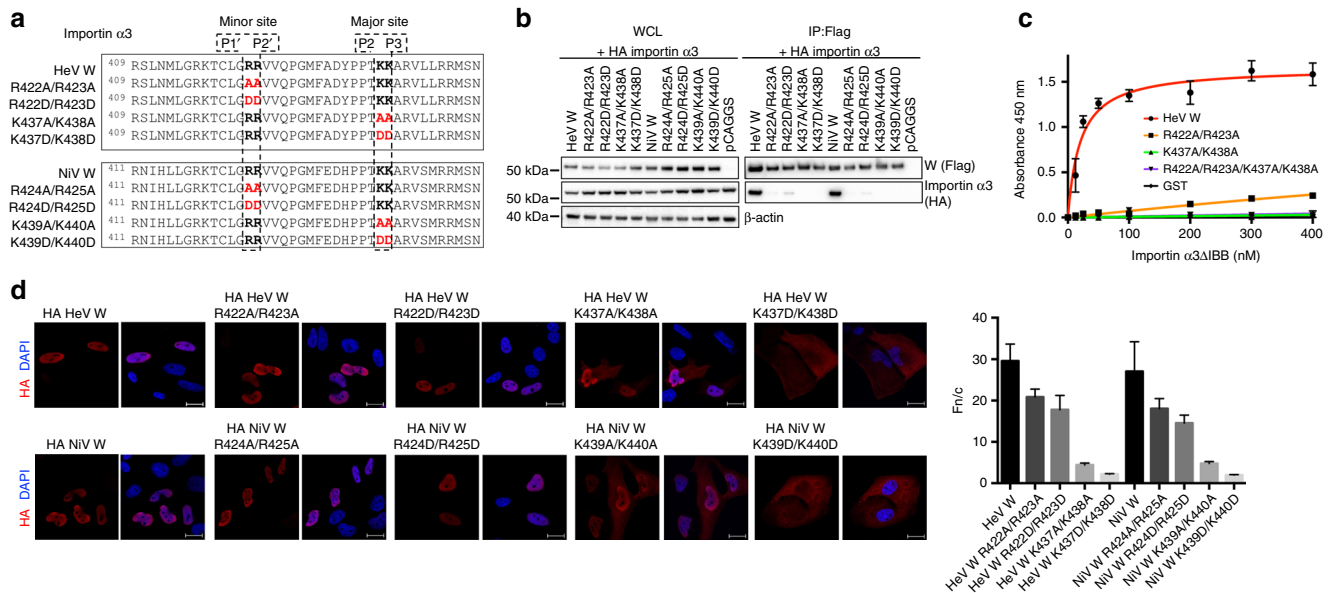


Fig. 4 Both importin $\alpha 3$ major and minor sites are important for the HeV NiV W protein interactions. **a** Schematic of the mutations made in the W protein to test the binding contributions to the major and minor binding sites for importin $\alpha 3$. **b** Co-immunoprecipitation assay performed with Flag antibody on lysates of HEK293T cells expressing HA-tagged importin $\alpha 3$ and Flag-tagged HeV W, NiV W, and mutant W constructs as indicated. Western blots were performed for HA and Flag. WCL, whole cell lysate; IP, immunoprecipitation. pCAGGS denotes empty vector control. **c** HeV W mutations were tested against importin $\alpha 3$ using the ELISA assay. GST-HeV W and mutants were coated on 96-well plates, and binding of 6xHis-tagged importin $\alpha 3$ assessed using an anti-6xHis HRP antibody. Error bars show the S.E.M for three replicates. **d** HeLa cells were transfected with indicated HA-tagged HeV and NiV W plasmids. Twenty-four hours post transfection, cells were fixed and stained with anti-HA antibody and Alexa Fluor 594 to visualise protein localisation. Image is representative. Scale bar depicted is 20 μ m. The ratio of nuclear to cytoplasmic fluorescence (Fn/c) was determined for 50 cells for each construct, error bars represent the SEM

shown to auto-inhibit differentially across isoforms¹⁹. However, our results identify clear differences in the structural positioning of the C-terminal ARM domains 7–8 of importin $\alpha 1$ and $\alpha 3$, accompanied with a significant increase in the binding interface at this region in importin $\alpha 3$. In addition, the chimeric protein importin $\alpha 1^{\text{ARM1-5}}\alpha 3^{\text{ARM6-10}}$ binds to W, whereas importin $\alpha 3^{\text{ARM1-5}}\alpha 1^{\text{ARM6-10}}$ does not interact, confirming that the C-terminal domain of the importin α is the differentiating factor, rather than the N terminus. The importance of the C-terminal ARM repeats has been demonstrated for importin $\alpha 5$ binding of nonclassical NLS cargo, involving a distinct mechanism and ARM repeat 10³⁸. It has also been hypothesised that that flexibility of importin $\alpha 3$ may mediate increased specificity and/or affinity, and indeed, this was described as a contributing factor to the binding of RCC1. However, this is unlikely to have a role in the specificity of importin $\alpha 3$ for the W protein, because the difference in binding interactions occur outside of the hinge region. As well, if the hinge region was critical for mediating specificity, the $\alpha 3^{\text{ARM1-5}}\alpha 1^{\text{ARM6-10}}$ chimera would have interacted with W if the hinge region was the critical region for mediating specificity. In addition, we show through structural comparisons between apo- and W bound-importin $\alpha 3$, that structural changes in the N terminus were not associated with direct binding interactions in this region. Importantly, these results do not discount the previous work of RCC1 binding, but rather, complement and extend it by highlighting that different mechanisms are likely to exist in mediating specificity.

Our study defines a basis to explain the importin α specificity of henipavirus HeV W and NiV W virulence factors for importins, demonstrating that differences in the ARM repeats in the C terminus of importin $\alpha 3$ mediate specificity. Nuclear transport of cargo in an isoform and tissue-specific manner is critical for health and disease. Subtype switching of importin $\alpha 1$ to $\alpha 5$ in

embryonic stem cells results in the initiation of neural differentiation³⁹, and the maintenance and lineage determination of embryonic stem cells⁴⁰. Differential expression of importin $\alpha 3$ has been demonstrated to occur following rabies infection, with overexpression observed only in paralytic rabies, suggesting a possible prognostic marker⁴¹. The inhibition of importin $\alpha 3$ has also been shown to attenuate prostate cancer metastasis⁴². The expanded rules for isoform specificity outlined here will provide important insights into our understanding of nuclear transport adaptor cargo specificity and their function in cellular processes.

Methods

Plasmids for recombinant protein expression. The C-terminal domain of HeV (residues 409–448; UniProtKB P0C1C6) and NiV (residues 411–450; UniProtKB P0C1C7) with an N-terminal TEV cleavage site (ENLYFQS) were codon optimised for expression in *Escherichia coli* and synthesised (Genscript, Piscataway, NJ). These constructs were cloned into pGEX4T-1 vector at BamHI and EcoRI sites. Importin $\alpha 3$ and $\alpha 7$ lacking the auto-inhibitory IBB domain (residues 64–521 and 73–536) were codon optimised for *E. coli* expression, synthesised and cloned into pET15b vector at NdeI and EcoRI sites. The importin α chimeras lacking the auto-inhibitory IBB domain (for recombinant expression) were comprised of $\alpha 1^{\text{aa71-279}}\alpha 3^{\text{aa271-521}}$ and $\alpha 3^{\text{aa64-270}}\alpha 1^{\text{aa280-529}}$, with numbering according to UniProtKB P52292 and UniProtKB O00629 for importin $\alpha 1$ and importin $\alpha 3$, respectively. Importin $\alpha 1\Delta$ IBB, encoding residues 71–529, was cloned in the pET30 vector as described previously^{43,44}.

Recombinant expression and purification. Plasmids were transformed into BL21 (DE3) pLysS cells and expressed using the Studier auto-induction method⁴⁵. In brief, starter cultures were inoculated into 2 L baffled flasks containing 500 mL of expression media consisting of 1% (w/v) tryptone, 0.5% (w/v) yeast extract, 0.5% glycerol, 0.05% glucose, 0.2% (w/v) α -lactose, 0.025 M NH_4SO_4 , 0.05 M KH_2PO_4 , 0.05 M Na_2HPO_4 , 1 mM magnesium chloride and either 100 $\mu\text{g}/\text{mL}$ ampicillin, or 50 $\mu\text{g}/\text{mL}$ kanamycin. Cells were harvested via centrifugation at 6500 \times g and 18 $^\circ\text{C}$ for 30 min and resuspended in phosphate buffer (PB) (20 mM imidazole, 300 mM NaCl, 50 mM phosphate pH 8.0) or Tris-buffered saline (TBS) (Tris pH 8.0, 125 mM NaCl) buffer with complete ethylenediaminetetraacetic acid (EDTA)-free

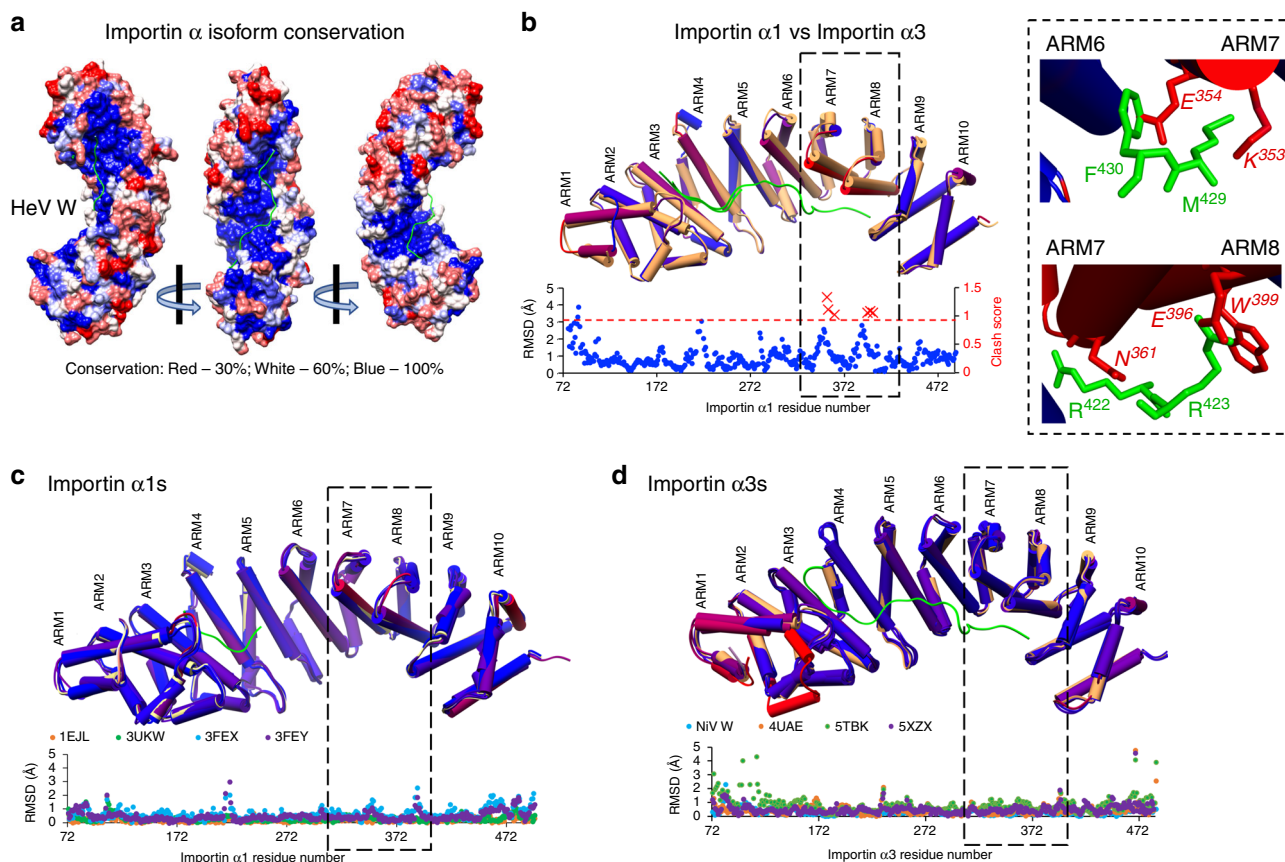


Fig. 5 Structural basis for specificity of Henipavirus W binding to the importin $\alpha 3$. **a** Importin $\alpha 3$:HeV W structure coloured by conservation of amino acids across all importin α isoforms highlights a 100% conservation in the binding interface. The HeV W NLS backbone (coloured green) is shown in complex with importin $\alpha 3$, with sequence colour rendering red at 30%, white 60%, and blue 100% sequence identity. Figure created in UCSF Chimera using importin α alignments from Clustal Omega. **b** To identify structural differences, the structures of importin $\alpha 1$:HeV W and importin $\alpha 3$:HeV W were superimposed in UCSF Chimera using MatchEnsemble, and r.m.s.d. plots generated using MatchAlign, and MatchAssess functions. α -helices shown as cylinders; importin $\alpha 3$ coloured orange throughout, and colour conservation rendering for importin $\alpha 1$ set for blue, < 2.5 \AA variance, and red for variances > 2.5 \AA . Molprobit was used to analyse clash data of importin $\alpha 3$:HeV W NLS superimposed to importin $\alpha 1$, all clashes > 0.8 shown as red crosses. Differences in clash score between importin $\alpha 1$ and $\alpha 3$ are localised to ARMs 7 and 8. Detailed view of clashes are presented in the right box, highlighting residues clashing with the W NLS owing to the difference in positioning of ARMs 7 and 8 in importin $\alpha 1$. All clashing residues are positioned on the α -helices of the ARMs. **c** Structural comparisons of importin $\alpha 1$ bound to a range of cargo was examined by superimposing the $\alpha 1$:HeV W NLS structure determined in this study (reference molecule, coloured yellow), with importin $\alpha 1$ bound to a monopartite SV40T NLS¹² (1EJL), bipartite Bimax NLS^{59,60} (3UKW), and two domain bound structures of CAP80⁶¹ (3FEX, 3FEY) coloured according to r.m.s.d as described in **b**. Positioning of the α -helices in ARMs 7 and 8 are relatively static across all structures. **d** Structural comparisons of importin $\alpha 3$ bound to a range of cargo was examined by superimposing the $\alpha 3$:HeV W NLS structure determined in this study (reference molecule coloured orange) with the monopartite RanBP3⁶² (5XZX), the NiV W (this study), and domains of PB2¹⁹ (4UAE) and RCC1¹⁵ (5TBK) coloured according to r.m.s.d as described in **b**. Positioning of α -helices in ARMs 7 and 8 are also relatively static across all structures

protease inhibitor. Cells were lysed using two freeze–thaw cycles and addition of 20 mg lysozyme and 0.5 mg DNase.

Affinity purifications of 6xHis-tagged importin α were performed by injecting clarified cell lysate onto a GE HisTrap 5 mL column using PB, washing the column with 15 column volumes and then eluting over 5 column volumes using a gradient elution with high imidazole PB (500 mM imidazole, 300 mM NaCl, 50 mM phosphate pH 8.0). Affinity purifications of GST-tagged proteins were performed on a GST Trap 5 mL column using TBS, and elution buffer containing 10 mM glutathione. All size exclusion purifications were performed on a Superdex 200 pg 26/600 column using TBS pH 8.0, and eluted proteins were pooled and concentrated using 10 kDa MW centrifuge filters. Complex formation was performed as described previously⁴⁶.

ELISA. The method was based on previously published microtiter plate assays⁴⁷. In brief, 96-well clear plates were coated with GST-NLS fusion proteins using bicarbonate/carbonate buffer pH 9.6 for 2 h at room temperature. The plates were washed using TBS containing 0.05% v/v Tween20 (TBST). Blocking was achieved using 5% (w/v) skim milk in TBST for 2 h at room temperature. Wells were washed three times in TBST buffer and incubated with decreasing concentrations of 6xHis-

tagged importin α (400, 300, 200, 100, 50, 25, 12.5 and 0 nM) diluted in TBS for 2 h. The plate was washed three times, blocked for 2 h, washed a further three times and then incubated for 2 h with 100 μ L of a 1/5000 dilution of anti-6xHis 4HRP conjugated rabbit polyclonal antibody (Abcam ab1187). The plate was washed a further three times before addition of 100 μ L of TMB substrate (Sigma T4444). The colorimetric reaction proceeded for 20 min before being stopped with 100 μ L of 2 M H₂SO₄, and the absorbance measured at 450 nm using an Epoch microplate spectrophotometer (Biotek). One-site specific binding analysis using least squares fit was performed using GraphPad Prism version 7.00 for Mac, GraphPad Software, La Jolla California USA, www.graphpad.com.

Microscale thermophoresis. Affinity measurements using MST were carried out employing a Monolith NT.115 instrument (NanoTemper Technologies)⁴⁸. Purified importin $\alpha 1$, $\alpha 3$ and $\alpha 7$ in 20 mM 4-(2-hydroxyethyl)-1-piperazineethanesulfonic acid (HEPES), 150 mM NaCl, pH 8.0 were labelled using the NHS RED NanoTemper labelling kit according to the manufacturer's instructions. For the assay, 5 μ L of labelled protein was mixed with 10 μ L of the unlabelled NiV W at various concentrations and 5 μ L of 0.05% (w/v) Tween20. All experiments were incubated for 10 min before applying samples to Monolith NT Standard Treated Capillaries

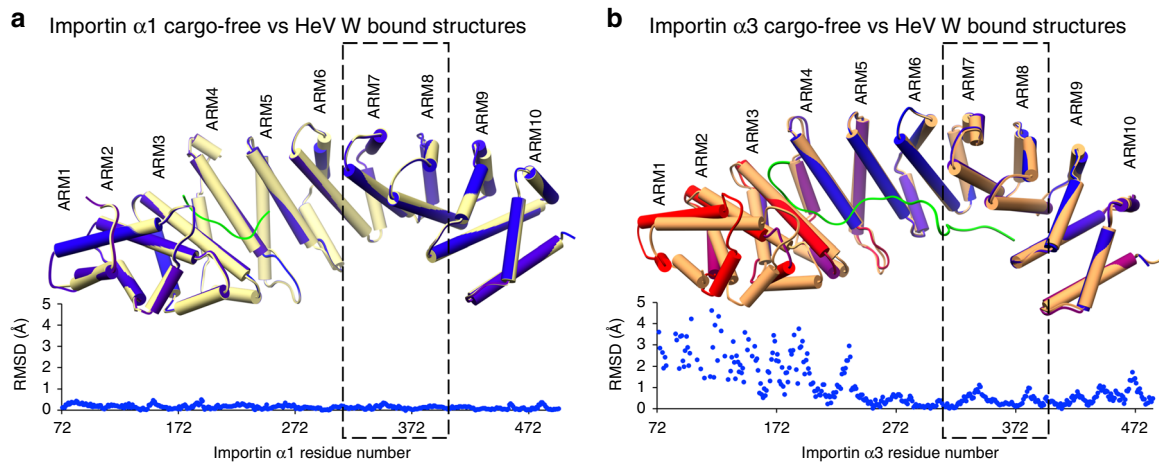


Fig. 6 Structures of cargo-free importin $\alpha 1$ and $\alpha 3$ confirm ARMs 7 and 8 positioning. **a** Importin $\alpha 1$ cargo-free structure and structural superposition with importin $\alpha 1$:HeV W complex (reference molecule, coloured yellow) and associated r.m.s.d plot. The positioning of the α -helices in ARM repeats 7 and 8 are static across all structures. The importin $\alpha 1$ is coloured by r.m.s.d rendering where blue < 2.5 Å variance, and red for variances above 2.5 Å. **b** Importin $\alpha 3$ cargo-free structure, together with the associated structural superposition with importin $\alpha 3$:HeV W complex, and r.m.s.d plot. Importin α structures were aligned in UCSF Chimera using MatchEnsemble, and r.m.s.d. plots were generated using MatchAlign, and MatchAssess functions. Colouring as per **a**, but with importin $\alpha 3$:HeV W in orange

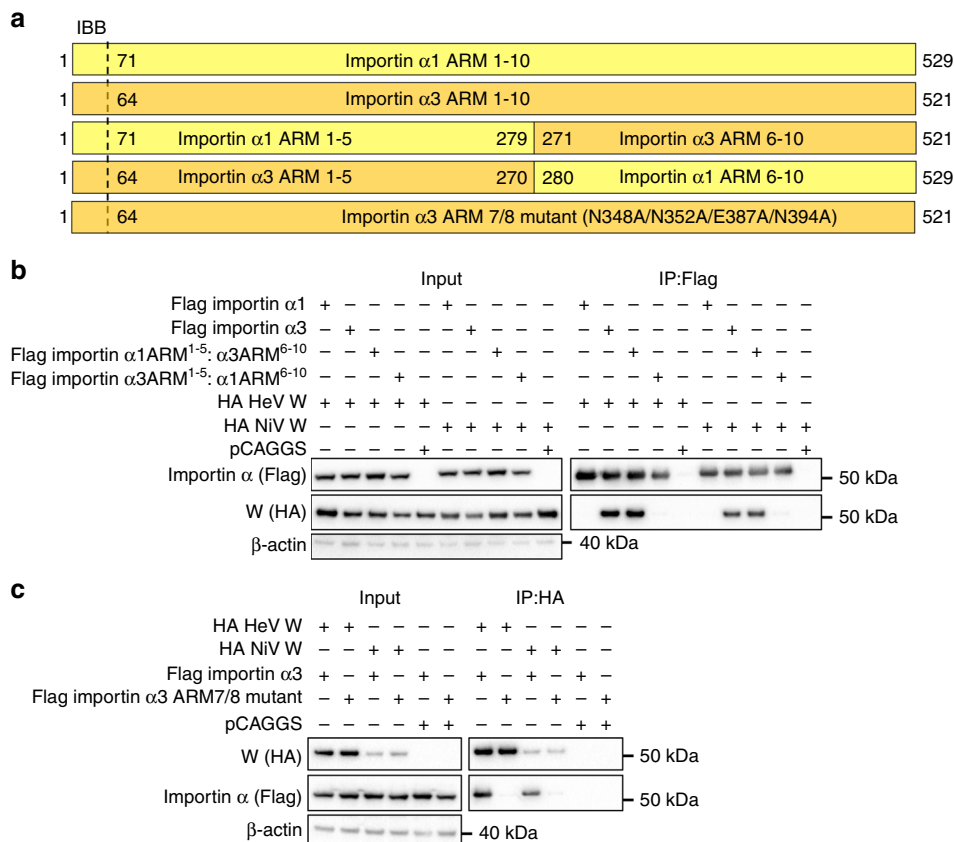


Fig. 7 Confirming the structural hypothesis through importin α chimeras. **a** Schematic representation of importin $\alpha 1$, $\alpha 3$, and chimeric importin $\alpha 1$ ARM¹⁻⁵: $\alpha 3$ ARM⁶⁻¹⁰ and importin $\alpha 3$ ARM¹⁻⁵: $\alpha 1$ ARM⁶⁻¹⁰ constructs. **b** Co-immunoprecipitation assay performed with Flag antibody on lysates of HEK293T cells expressing Flag-tagged importin $\alpha 1$, $\alpha 3$, importin $\alpha 1$ ARM¹⁻⁵: $\alpha 3$ ARM⁶⁻¹⁰ and importin $\alpha 3$ ARM¹⁻⁵: $\alpha 1$ ARM⁶⁻¹⁰, and HA-tagged HeV W and NiV W, as indicated. Western blots were performed for HA and Flag. WCL, whole cell lysate; IP, immunoprecipitation. pCAGGS denotes empty vector control. **c** Co-immunoprecipitation assay performed with HA antibody on lysates of HEK293T cells expressing Flag-tagged importin $\alpha 1$, $\alpha 3$, importin $\alpha 1$ ARM¹⁻⁵: $\alpha 3$ ARM⁶⁻¹⁰ and importin $\alpha 3$ ARM¹⁻⁵: $\alpha 1$ ARM⁶⁻¹⁰, and HA-tagged HeV W and NiV W, as indicated. Western blots were performed for HA and Flag. WCL, whole-cell lysate; IP, immunoprecipitation. pCAGGS denotes empty vector control

(NanoTemper Technologies). Thermophoresis was measured at 25 °C with laser off/on/off times of 5 s/30 s/5 s. Experiments were conducted at 20% light-emitting diode power and 20–40% MST infra-red laser power. Data from three independently performed experiments were fitted to the single binding model via the NT. Analysis software version 1.5.41 (NanoTemper Technologies) using the signal from Thermophoresis + T-Jump.

Crystallisation. All crystals were obtained using the hanging drop vapour diffusion method over a 300 µL reservoir solution. Importin $\alpha 1\Delta$ IBB was crystallised with 1 M NH_4SO_4 , 0.01 M DTT, 0.1 M sodium HEPES pH 7.0. The importin $\alpha 1\Delta$ IBB:NiV W and importin $\alpha 1\Delta$ IBB:HeV W complexes were crystallised in 0.01 M DTT, 0.7 M sodium citrate and 0.1 M sodium HEPES pH 7.0, with rod-shaped crystals forming within 2–3 days. Importin $\alpha 3\Delta$ IBB was crystallised using 0.2 M sodium nitrate, 0.1 M Bis-Tris propane pH 6.5 and 25% (w/v) PEG 3350. Plate-like crystals formed within 2–3 weeks. The importin $\alpha 3\Delta$ IBB:NiV W complex crystallised in 0.2 M lithium nitrate, 20% (w/v) PEG 3350 conditions with a rod morphology that diffracted to 2.3 Å. The importin $\alpha 3\Delta$ IBB:HeV W complex crystallised in three forms. Crystal form 1 was obtained using 0.1 M sodium citrate pH 5.0 and 20% (w/v) PEG 2000, crystal form 2 was obtained using 0.1 M sodium HEPES pH 7.5, 25% (w/v) PEG 200 MME and crystal form 3 obtained using 0.2 M sodium chloride, 0.1 M MES pH 6.5, 10% (w/v) PEG 4000 conditions. Diffraction of the importin $\alpha 3\Delta$ IBB:HeV W complex crystal forms ranged from 1.6–2.3 Å.

Data collection and processing. X-ray diffraction data were collected at the Australian Synchrotron on the MX1⁴⁹ and MX2⁵⁰ macromolecular beam lines using an ASDC Quantum 210r, ASDC Quantum 315r detector and Eiger 16 M detector, respectively. Data reduction and integration was performed using iMosflm⁵¹ for data collected using ADSC 210r and ADSC 315r detectors, whereas reduction and integration of data collected on Eiger 16 M was performed using XDS⁵². Merging, space group assignment, scaling and selection of 5% reflections for R_{free} calculations was done using Aimless^{53,54} and the CCP4 suite⁵⁵. Phasing was performed using molecular replacement in Phaser MR⁵⁶, with PDBID 5FC8 used as a search model for importin $\alpha 1$ cargo-free, importin $\alpha 1$:HeV W complex and importin $\alpha 1$:NiV W. The importin $\alpha 3$:HeV W complex was phased using 4UAE as a search model, from which the solution was then used as a search model for the importin $\alpha 3$:NiV W complex. The cargo-free importin $\alpha 3$ structure was phased by placing the N terminus and C terminus domains separately. Models were refined using iterative cycles of manual real space coot⁵⁷ and maximum likelihood phenix refine⁵⁸.

Cell culture and plasmids. HEK293T (ATCC—CRL-3216) and Hela cells (ATCC—CCL-2) were maintained in Dulbecco's Modified Eagle Medium, supplemented with 10% fetal bovine serum and cultured at 37 °C and 5% CO_2 .

The sequence for HeV W (NCBI: JN255804.1) was synthesised (Genscript, Piscataway, NJ) and cloned with N-terminal Flag- and HA-tags into the mammalian expression plasmid pCAGGS. pCAGGS HA NiV W was previously described²⁰. NiV W was subcloned with a Flag-tag into pCAGGS. Overlapping PCR was used to clone HeV W R422A/R423A, HeV W R422D/R423D, HeV W K437A/K438A, HeV W K437D/K438D, NiV W R424A/R425A, NiV W R424D/R425D, NiV W K439A/K440A, NiV W K439D/K440D and importin $\alpha 3$ ARMs 7/8 mutant (N348 A/N352A/E387A/N394A), which were then cloned with an HA- or Flag-tag into pCAGGS. pCAGGS Flag importin $\alpha 1$, $\alpha 3$, $\alpha 4$, $\alpha 5$, $\alpha 6$ and $\alpha 7$ were previously described^{20,36}. Importin $\alpha 3$ was subcloned with an HA-tag into pCAGGS. Overlapping PCR was used to generate the chimeric importin $\alpha 1^{\text{ARM1-5}}$: $\alpha 3^{\text{ARM6-10}}$ (residues 1–279 of importin $\alpha 1$ and residues 271–521 of importin $\alpha 3$) and importin $\alpha 3^{\text{ARM1-5}}$: $\alpha 1^{\text{ARM6-10}}$ (residues 1–270 of importin $\alpha 3$ and residues 280–529 of importin $\alpha 1$), which were cloned with Flag tags into pCAGGS. For additional information regarding primers used in this study, please see Supplementary Table 6.

Co-immunoprecipitation assays. HEK293T cells (1×10^6) were transfected with the indicated plasmids using Lipofectamine 2000 (Thermo Fisher Scientific, MA) and at 24 h post transfection, cells were lysed in NP-40 lysis buffer (50 mM Tris pH 7.5, 280 mM NaCl, 0.5% Nonidet P-40, 0.2 mM EDTA, 2 mM ethylene glycol-bis(β -aminoethyl ether)-N,N,N',N'-tetraacetic acid, 10% glycerol, protease inhibitor (complete; Roche, Indianapolis, IN)). Anti-FLAG M2 magnetic beads or EZview Red anti-HA Agarose affinity gel (Sigma-Aldrich, St. Louis, MO) were incubated as indicated with lysates for 1 h at 4 °C, washed five times in NP-40 lysis buffer, and eluted using 3X FLAG or HA peptide (Sigma-Aldrich, St. Louis, MO) at 4 °C for 30 min. Whole cell lysates and co-precipitation samples were analysed by western blot.

Immunofluorescence. Hela cells (3×10^4) grown on glass coverslips were transfected with indicated HeV and NiV W plasmids (300 ng) using Lipofectamine 2000 (Thermo Fisher Scientific, MA). At 24 h post transfection, cells were fixed using 4% paraformaldehyde and permeabilised using 0.1% Triton X-100. Cells were stained using mouse anti-HA (H3663, Sigma-Aldrich, MO) (dilution 1:500) and secondary antibody conjugated to Alexa Fluor 594 (A-11032, Thermo Fisher Scientific, MA) (dilution 1:2000). Images were taken using a Zeiss LSM 800 confocal microscope at $\times 64$. To determine the ratio of nuclear to cytoplasmic fluorescence signal (Fn/c),

Hela cells (1×10^4) were plated in a 96-well plate (black, clear bottom, Corning) and transfected with the indicated HeV and NiV W plasmids (300 ng) using Lipofectamine 2000. At 24 h post transfection, cells were fixed and permeabilised as above and stained with anti-HA (H6908, Sigma-Aldrich, MO) (dilution 1:500) and Alexa Fluor 488 (A32731, Thermo Fisher Scientific, MA) (dilution 1:2000). Images were taken at $\times 10$ using a BioTek Cytation 5 Cell Imaging Multi-Mode reader and were analysed using Gen5 Image Prime software to determine Fn/c, using the calculation $\text{Fn/c} = (\text{Fn-background})/(\text{Fc-background})$, where Fn is nuclear fluorescence and Fc is cytoplasmic fluorescence. Fn/c was determined for 50 cells in each condition; error bars indicate the standard error of the mean (SEM).

Antibodies. Polyclonal rabbit anti-Flag (F7425), polyclonal rabbit anti-HA (H6908), and monoclonal mouse anti-HA (H3663) were purchased from Sigma-Aldrich (St. Louis, MO). Monoclonal rabbit β -actin antibody was purchased from Cell Signalling (4967 S) (Danvers, MA).

Western blots. Lysates were run on 10% Bis-Tris Plus polyacrylamide gels (Thermo Fisher Scientific, MA) and transferred to polyvinylidene difluoride membrane (Bio-Rad, Hercules, CA). Membranes were probed with the indicated antibodies and were developed using Western Lightning Plus ECL (Perkin Elmer, Waltham, MA) and imaged using a ChemiDoc MP Imaging System (Bio-Rad, Hercules, CA).

GST pull-down assay. Each binding experiment was comprised of 100 µL of 30 µM GST or GST-SV40Tag, combined with 100 µL of 30 µM of each importin a variant, and incubated at room temperature for 2 h with 50 µL of glutathione agarose beads (Sigma G4510). The beads were centrifuged and washed three times with 1 mL Tris wash buffer (125 mM NaCl, Tris pH 8.0). Samples were centrifuged, the supernatant discarded, and 50 µL sodium dodecyl sulfate polyacrylamide gel electrophoresis (SDS-PAGE) loading buffer containing 100 mM DTT was added to each tube. Samples were heated for 10 min at 95 °C, vortexed for 5 min, centrifuged for 10 min at $17\,000 \times g$ and analysed by SDS-PAGE (165 V for 30 min on a 4–12% Bis-Tris plus gel (Novagen)).

Data availability

Atomic coordinates and related structure factors have been deposited to the Protein Data Bank with accession codes 6BW1, 6BW0, 6BW9, 6BWA, 6BWB, 6BVV, 6BVT and 6BVZ for the importin $\alpha 1$:HeV W ($P2_1, 2_1$ space group), importin $\alpha 1$:NiV W ($P2_1, 2_1$ space group), importin $\alpha 3$:HeV W crystal form 1 ($P12_1$ space group), importin $\alpha 3$:HeV W crystal form 2 ($P12_1$ space group), importin $\alpha 3$:HeV W crystal form 3 ($P2_1, 2_1$ space group), importin $\alpha 3$:NiV W ($P12_1$ space group), importin $\alpha 1$ ($P2_1, 2_1$ space group), importin $\alpha 3$ ($P12_1$ space group), respectively. All other data that support the findings of this study are available from the corresponding authors on reasonable request.

Received: 21 December 2017 Accepted: 29 June 2018

Published online: 12 September 2018

References

- Macara, I. G. Transport into and out of the nucleus. *Microbiol. Mol. Biol. Rev.* **65**, 570–594 (2001).
- Bednenko, J., Cingolani, G. & Gerace, L. Nucleocytoplasmic transport: navigating the channel. *Traffic* **4**, 127–135 (2003).
- Stewart, M. Molecular mechanism of the nuclear protein import cycle. *Nat. Rev. Mol. Cell Biol.* **8**, 195–208 (2007).
- Goldfarb, D. S., Corbett, A. H., Mason, D. A., Harreman, M. T. & Adam, S. A. Importin alpha: a multipurpose nuclear-transport receptor. *Trends. Cell Biol.* **14**, 505–514 (2004).
- Cingolani, G., Petosa, C., Weis, K. & Müller, C. W. Structure of importin- β bound to the IBB domain of importin- α . *Nature* **399**, 221–229 (1999).
- Milles, S. et al. Plasticity of an ultrafast interaction between nucleoporins and nuclear transport receptors. *Cell* **163**, 734–745 (2015).
- Lee, S. J., Matsuura, Y., Liu, S. M. & Stewart, M. Structural basis for nuclear import complex dissociation by RanGTP. *Nature* **435**, 693–696 (2005).
- Moroianu, J., Blobel, G. & Radu, A. Nuclear protein import: Ran-GTP dissociates the karyopherin alpha heterodimer by displacing alpha from an overlapping binding site on beta. *Proc. Natl. Acad. Sci.* **93**, 7059–7062 (1996).
- Kutay, U., Bischoff, F. R., Kostka, S., Kraft, R. & Görlich, D. Export of importin alpha from the nucleus is mediated by a specific nuclear transport factor. *Cell* **90**, 1061–1071 (1997).
- Bischoff, F. R. & Görlich, D. RanBP1 is crucial for the release of RanGTP from importin β -related nuclear transport factors. *FEBS Lett.* **419**, 249–254 (1997).

11. Kobe, B. Autoinhibition by an internal nuclear localization signal revealed by the crystal structure of mammalian importin α . *Nat. Struct. Mol. Biol.* **6**, 388–397 (1999).
12. Fontes, M. R., Teh, T. & Kobe, B. Structural basis of recognition of monopartite and bipartite nuclear localization sequences by mammalian importin- α . *J. Mol. Biol.* **297**, 1183–1194 (2000).
13. Chen, M.-H. et al. Phospholipid scramblase 1 contains a nonclassical nuclear localization signal with unique binding site in importin α . *J. Biol. Chem.* **280**, 10599–10606 (2005).
14. Giesecke, A. & Stewart, M. Novel binding of the mitotic regulator TPX2 (target protein for *Xenopus* kinesin-like protein 2) to importin- α . *J. Biol. Chem.* **285**, 17628–17635 (2010).
15. Sankhala, R. S. et al. Three-dimensional context rather than NLS amino acid sequence determines importin α subtype specificity for RCC1. *Nat. Commun.* **8**, 979 (2017).
16. Ao, Z. et al. Importin $\alpha 3$ interacts with HIV-1 integrase and contributes to HIV-1 nuclear import and replication. *J. Virol.* **84**, 8650–8663 (2010).
17. Xu, W. et al. Ebola virus VP24 targets a unique NLS binding site on karyopherin alpha 5 to selectively compete with nuclear import of phosphorylated STAT1. *Cell Host. Microbe* **16**, 187–200 (2014).
18. Nardozzi, J., Wenta, N., Yasuhara, N., Vinkemeier, U. & Cingolani, G. Molecular basis for the recognition of phosphorylated STAT1 by importin $\alpha 5$. *J. Mol. Biol.* **402**, 83–100 (2010).
19. Pumroy, R. A., Ke, S., Hart, D. J., Zachariae, U. & Cingolani, G. Molecular determinants for nuclear import of influenza A PB2 by importin α isoforms 3 and 7. *Structure* **23**, 374–384 (2015).
20. Shaw, M. L., Cardenas, W. B., Zamarin, D., Palese, P. & Basler, C. F. Nuclear localization of the Nipah virus W protein allows for inhibition of both virus- and toll-like receptor 3-triggered signaling pathways. *J. Virol.* **79**, 6078–6088 (2005).
21. Audsley, M. D., Jans, D. A. & Moseley, G. W. Nucleocytoplasmic trafficking of Nipah virus W protein involves multiple discrete interactions with the nuclear import and export machinery. *Biochem. Biophys. Res. Commun.* **479**, 429–433 (2016).
22. Eaton, B. T., Broder, C. C., Middleton, D. & Wang, L.-F. Hendra and Nipah viruses: different and dangerous. *Nat. Rev. Microbiol.* **4**, 23–35 (2006).
23. Kulkarni, S. et al. Nipah virus edits its P gene at high frequency to express the V and W proteins. *J. Virol.* **83**, 3982–3987 (2009).
24. Wang, L.-F. et al. Molecular biology of Hendra and Nipah viruses. *Microbes Infect.* **3**, 279–287 (2001).
25. Lo, M. K. et al. Determination of the henipavirus phosphoprotein gene mRNA editing frequencies and detection of the C, V and W proteins of Nipah virus in virus-infected cells. *J. Gen. Virol.* **90**, 398–404 (2009).
26. Shaw, M. L., Garcia-Sastre, A., Palese, P. & Basler, C. F. Nipah virus V and W proteins have a common STAT1-binding domain yet inhibit STAT1 activation from the cytoplasmic and nuclear compartments, respectively. *J. Virol.* **78**, 5633–5641 (2004).
27. Satterfield, B. A. et al. The immunomodulating V and W proteins of Nipah virus determine disease course. *Nat. Commun.* **6**, 7483 (2015).
28. Satterfield, B. A. et al. The Nipah virus C and W proteins contribute to respiratory disease in ferrets. *J. Virol.* **JVI**, 00215–00216 (2016).
29. Yoneda, M. et al. The nonstructural proteins of Nipah virus play a key role in pathogenicity in experimentally infected animals. *PLoS ONE* **5**, e12709 (2010).
30. Lo, M. K. et al. Characterization of the antiviral and inflammatory responses against Nipah virus in endothelial cells and neurons. *Virology* **404**, 78–88 (2010).
31. Martinez-Gil, L., Vera-Velasco, N. M. & Mingarro, I. Exploring the human-Nipah virus protein-protein interactome. *J. Virol.* **91**, e01461–01417 (2017).
32. Ciancanelli, M. J., Volchkova, V. A., Shaw, M. L., Volchkov, V. E. & Basler, C. F. Nipah virus sequesters inactive STAT1 in the nucleus via a P gene-encoded mechanism. *J. Virol.* **83**, 7828–7841 (2009).
33. Miyatake, H. et al. Crystal structure of human importin- $\alpha 1$ (Rch1), revealing a potential autoinhibition mode involving homodimerization. *PLoS ONE* **10**, e0115995 (2015).
34. Welch, K., Franke, J., Kohler, M. & Macara, I. G. RanBP3 contains an unusual nuclear localization signal that is imported preferentially by importin $\alpha 3$. *Mol. Cell Biol.* **19**, 8400–8411 (1999).
35. Fagerlund, R., Kinnunen, L., Kohler, M., Julkunen, I. & Melen, K. NF- κ B is transported into the nucleus by importin $\alpha 3$ and importin $\alpha 4$. *J. Biol. Chem.* **280**, 15942–15951 (2005).
36. Reid, S. P., Valmas, C., Martinez, O., Sanchez, F. M. & Basler, C. F. Ebola virus VP24 proteins inhibit the interaction of NPI-1 subfamily karyopherin alpha proteins with activated STAT1. *J. Virol.* **81**, 13469–13477 (2007).
37. Gabriel, G. et al. Differential use of importin- α isoforms governs cell tropism and host adaptation of influenza virus. *Nat. Commun.* **2**, 156 (2011).
38. Nardozzi, J. D., Lott, K. & Cingolani, G. Phosphorylation meets nuclear import: a review. *Cell Commun. Signal.* **8**, 32 (2010).
39. Yasuhara, N. et al. Triggering neural differentiation of ES cells by subtype switching of importin- α . *Nat. Cell Biol.* **9**, 72–79 (2007).
40. Yasuhara, N. & Yoneda, Y. Importins in the maintenance and lineage commitment of ES cells. *Neurochem. Int.* (2017).
41. Venugopal, A. K. et al. Quantitative proteomics for identifying biomarkers for Rabies. *Clin. Proteom.* **10**, 3 (2013).
42. Yang, J. et al. Inhibition of KPNA4 attenuates prostate cancer metastasis. *Oncogene* **36**, 2868–2878 (2017).
43. Teh, T., Tiganis, T. & Kobe, B. Crystallization of importin α , the nuclear-import receptor. *Acta Crystallogr. D Biol. Crystallogr.* **55**, 561–563 (1999).
44. Marfori, M. et al. Molecular basis for specificity of nuclear import and prediction of nuclear localization. *Biochim. Et. Biophys. Acta* **1813**, 1562–1577 (2011).
45. Studier, F. W. Protein production by auto-induction in high-density shaking cultures. *Protein Expr. Purif.* **41**, 207–234 (2005).
46. Smith, K. M. et al. Contribution of the residue at position 4 within classical nuclear localization signals to modulating interaction with importins and nuclear targeting. *Biochim. Biophys. Acta* **1865**, 1114–1129 (2018).
47. Chaston, J. J., Stewart, A. G. & Christie, M. Structural characterisation of TNRC6A nuclear localisation signal in complex with importin- α . *PLoS ONE* **12**, e0183587 (2017).
48. da Costa, T. P. S. et al. Structural determinants defining the allosteric inhibition of an essential antibiotic target. *Structure* **24**, 1282–1291 (2016).
49. Cowieson, N. P. et al. MX1: a bending-magnet crystallography beamline serving both chemical and macromolecular crystallography communities at the Australian Synchrotron. *J. Synchrotron Radiat.* **22**, 187–190 (2015).
50. Aragão, D. et al. MX2: a high-flux undulator microfocus beamline serving both the chemical and macromolecular crystallography communities at the Australian Synchrotron. *Synchrotron Radiat.* **25**, 885–891 (2018).
51. Battye, T. G. G., Kontogiannis, L., Johnson, O., Powell, H. R. & Leslie, A. G. W. iMOSFLM: a new graphical interface for diffraction-image processing with MOSFLM. *Acta Crystallogr. D Biol. Crystallogr.* **67**, 271–281 (2011).
52. Kabsch, W. XDS. *Acta Crystallogr. D Biol. Crystallogr.* **66**, 125–132 (2010).
53. Evans, P. R. An introduction to data reduction: space-group determination, scaling and intensity statistics. *Acta Crystallogr. D Biol. Crystallogr.* **67**, 282–292 (2011).
54. Evans, P. Scaling and assessment of data quality. *Acta Crystallogr. D Biol. Crystallogr.* **62**, 72–82 (2006).
55. Winn, M. D. et al. Overview of the CCP4 suite and current developments. *Acta Crystallogr. D Biol. Crystallogr.* **67**, 235–242 (2011).
56. McCoy, A. J. et al. Phaser crystallographic software. *J. Appl. Crystallogr.* **40**, 658–674 (2007).
57. Emsley, P., Lohkamp, B., Scott, W. G. & Cowtan, K. Features and development of Coot. *Acta Crystallogr. D Biol. Crystallogr.* **66**, 486–501 (2010).
58. Adams, P. D. et al. PHENIX: a comprehensive python-based system for macromolecular structure solution. *Acta Crystallogr. D Biol. Crystallogr.* **66**, 213–221 (2010).
59. Kosugi, S. et al. Design of peptide inhibitors for the importin α/β nuclear import pathway by activity-based profiling. *Chem. Biol.* **15**, 940–949 (2008).
60. Marfori, M., Lonhienne, T. G., Forwood, J. K. & Kobe, B. Structural basis of high-affinity nuclear localization signal interactions with importin - α . *Traffic* **13**, 532–548 (2012).
61. Dias, S. M., Wilson, K. F., Rojas, K. S., Ambrosio, A. L. & Cerione, R. A. The molecular basis for the regulation of the cap-binding complex by the importins. *Nat. Struct. Mol. Biol.* **16**, 930–937 (2009).
62. Koyama, M. & Matsuura, Y. Crystal structure of importin- $\alpha 3$ bound to the nuclear localization signal of Ran-binding protein 3. *Biochem. Biophys. Res. Commun.* **491**, 609–613 (2017).

Acknowledgements

Funding from NIH grants U19AI109664 and U19AI109945 assisted this work. This research was undertaken in part using the MX2 beamline at the Australian Synchrotron, part of ANSTO, and made use of the Australian Cancer Research Foundation (ACRF) Detector. Tpsc is supported by an NHMRC Fellowship (APP1091976). We also acknowledge the La Trobe University-Comprehensive Proteomics Platform for providing infrastructure. CFB is a Georgia Research Alliance Eminent Scholar in Microbial Pathogenesis. ST and EC were supported through a Graham Centre scholarship.

Author contributions

K.M.S. performed protein expression, purification, crystallisation, structure determination, structure analysis and manuscript preparation, S.T. performed protein expression, purification, crystallisation, structure determination and manuscript preparation, M.R.E. performed cloning, pull-down and nuclear import experiments, and manuscript preparation, J.B. performed cloning, T.P.S.C. performed MST experiments, D.A. assisted with data collection and structure determination, E.M.C. performed protein expression,

purification, crystallisation, C.F.B. performed experiment design and analysis and manuscript preparation, J.K.F. performed structure determination and manuscript preparation.

Additional information

Supplementary Information accompanies this paper at <https://doi.org/10.1038/s41467-018-05928-5>.

Competing interests: The authors declare no competing interests.

Reprints and permission information is available online at <http://npg.nature.com/reprintsandpermissions/>

Publisher's note: Springer Nature remains neutral with regard to jurisdictional claims in published maps and institutional affiliations.



Open Access This article is licensed under a Creative Commons Attribution 4.0 International License, which permits use, sharing, adaptation, distribution and reproduction in any medium or format, as long as you give appropriate credit to the original author(s) and the source, provide a link to the Creative Commons license, and indicate if changes were made. The images or other third party material in this article are included in the article's Creative Commons license, unless indicated otherwise in a credit line to the material. If material is not included in the article's Creative Commons license and your intended use is not permitted by statutory regulation or exceeds the permitted use, you will need to obtain permission directly from the copyright holder. To view a copy of this license, visit <http://creativecommons.org/licenses/by/4.0/>.

© The Author(s) 2018